# Semester Long Internship report

on

# Study of the effect of Drag correlations on Multiphase Eulerian-Eulerian Flow simulations

Submitted by

**M Siva Karthikeya**

Department of Aerospace Engineering

SASTRA Deemed University, Thanjavur, Tamilnadu, India

Under the guidance of

**Prof. Janani Srree Murallidharan,**

Assistant Professor, Department of Mechanical Engineering

IIT Bombay

# Acknowledgements

First and foremost, it is pleasant duty to express a deep sense of gratitude to **Prof. Kannan M Moudgalya**, IIT Bombay, for the initiative of Semester Long Internship program and providing students with a wonderful opportunity to carry out their project work at FOSSEE.

With immense pleasure, I would like to express my profound feelings of gratitude and obligation to my guide and project supervisor **Prof. Janani Srree Murallidharan,** Assistant Professor, IIT Bombay, for her priceless consolation, recommendations and support on every phase and for providing me an unmatchable experience throughout this project work.

I thank FOSSEE, IIT Bombay and the CFD team in particular for giving me the opportunity to work on this project. My sincere thanks to **Mr. Ashley Melvin** and **Mr. Divyesh Variya** for being extremely supportive at every stage and helping me navigate every step of the way throughout the course of this project work. **Mrs. Swetha Manian Sridhar** for the dedicated curating, structured organisation of this internship and ready response to our queries. **Dr. Anamika** and **Dr. Jayachandran** for their crucial inputs during the course of the project work.

Finally, I would like to thank all the faculty members, project advisors of our Institution and IIT Bombay, service people arranged by the management and our beloved parents and friends for supporting me to complete this work.

# Table of Contents

# List of Figures

# List of Tables

# Abstract

This project looks to study the effect of drag models on the CFD simulations for two very different and distinct industrial applications; one for the petroleum sector and the other the medical sector. The goal is to see if one drag model performs best across both these applications. A Eulerian-Eulerian approach is adopted and multi-fluid modelling method is used to understand the effect of multiple correlations adopted to model drag force, a predominant contributor to the momentum exchange between the two phases. OpenFOAM, an open-source CFD toolbox was employed to simulate both single and multiphase flows using the inbuilt simpleFoam and twoPhaseEulerFoam solver respectively. A fluidised bed is chosen as representative petroleum industry-based problem. For the CFD simulation, gas-solid Fluidized bed geometry is chosen to investigate the effect of various drag correlations on flow structure for accurate computational modelling of "Dispersed Multiphase flows". Multiphase simulations for multiple drag correlations identified Syamlal O'Brien drag closure to outperform other drag closures in accurately modelling a Dispersed Multiphase flow in fluidised bed. For the medical sector, the problem of blood plasma extraction was chosen. The present study involves first simulating blood as single phase in microfluidic chips with different microchannel structures so as to identify an efficient microchannel geometry to extract plasma by the hydrodynamic mechanism of Zweifach–Fung effect, the plasma- skimming effect, and the geometry effects induced by the microchannel design. Results from the single-phase study showed the Microchannel with a converging bent inlet (Type 3) to be more efficient in extracting plasma at a higher flow rate. As a continuation to this study, the newly identified geometry is used for multiphase simulations of blood, wherein the RBCs (Dispersed phase) and Plasma (continuous phase) will take to be two distinct phases. A lower hematocrit blood flow is established in the in the Type 3 microchannel such that pure plasma enters through 80% of the inlet and mixed plasma (RBC+Plasma) enters through the remaining 20% inlet.

# CHAPTER 1
# INTRODUCTION

## 1.1 OVERVIEW

Multiphase flows frequently occur in nature and in a multitude of other settings. They are of academic interest as well as are found in a wide scope of engineering applications, proceeding to pose a challenge to many research scientists and industrial practitioners alike. The efforts to understand fundamental behaviour and mechanisms of multiphase flow are necessarily a continuing process despite many important breakthroughs that have been made in the past.

As CPU's become more powerful and affordable, the usage of Computational Fluid Dynamics (CFD) is widely spread today to model any kind of phenomena occurring in nature to gain a fundamental understanding of the science behind it. But the mere availability of computational power is not going to guarantee the success of a simulation unless every parameter that contributes to the happening of a phenomenon in nature is taken into account. It is not a one-step procedure but an extensively iterative one.

Multiphase flow being one such phenomenon, requires immense computational power for modelling and a consideration of many minuscule parameters that can have a substantial impact on the end results. It is always challenging, yet fascinating to develop models that can replicate a realistic multiphase flow with immense accuracy.

Present study deals with one such minuscule parameter that is capable of converging the experimental results with the computational ones if modelled rightly. This is applied to a widely observed category of a Multiphase flow, the Dispersed Multiphase flow. The effect of altering this parameter in a Dispersed Multiphase flow belonging to two completely distinct and different industrial sectors is the ultimate goal of this research study.

## 1.2 SCOPE OF WORK

This sub-section outlines the scope of the project carried out based on the progress and discussions made so far.

The objective of this project at the infant stage has been to conduct studies on Dispersed Multiphase flows to accurately capture the phenomena occurring at the interface of the Continuous and Dispersed phases. Since momentum exchange between the phases is an important phenomenon that affects the flow structure at the interface, a thorough literature study was conducted to identify the factors that define this exchange process in a multiphase model.

The literature study helped in identifying Drag force as the predominant contributor of momentum exchange in a Dispersed Multiphase flow among other terms like the virtual mass force, life force and a few more [1]. This finding about the drag force propelled the project further to identify various drag correlations available in the literature that are suitable for modelling the desired flow.

After a rigorous study of various models that are readily coded in the open-source CFD toolbox, OpenFOAM, a clear-cut classification was made on the capability of each drag correlation on the basis of their operating range of voidage/packing fraction. Three drag models that are capable of modelling the flow over the entire range of packing fractions (0 to 1) are shortlisted for further study.

A 2D gas-solid fluidized bed, primarily belonging to the petroleum industry was considered the most suitable case to implement the chosen drag models for the reasons mentioned below.

1. Standard case of a dispersed multiphase flow
2. Availability of reliable experimental data to validate
3. Computationally less expensive for a Multiphase simulation

Conclusive results were obtained from the fluidized bed study on the efficiency of the three drag correlations in modelling a Dispersed Multiphase flow in the petroleum domain. The study is extended further to evaluate the performance of the drag correlations in the medical sector with the Backward facing step Microchannels, a compact and a convenient instrument for easy plasma extraction from the blood. A single-phase study was conducted on three design variants of the microchannel to identify the best geometry for efficient plasma extraction and a novel Type III variant displayed the desired characteristics.

Further, this newly identified geometry was used for multiphase simulations of blood, wherein the RBCs (Dispersed phase) and Plasma (continuous phase) will take to be two distinct phases. A lower hematocrit blood flow is established in the in the Type 3 microchannel such that pure plasma enters through 80% of the inlet and mixed plasma (RBC+Plasma) enters through the remaining 20% inlet.

## 1.3 MOTIVATION

Research on sustainable technologies has burgeoned in the 21st century to tackle environmental degradation occurring at every stage of any industrial process. Fluidized bed technology is one such potential deployment into the category of sustainable technologies, widely used in the petroleum, pharmaceutical, chemical, and many other industries and has been at a focal point of research. With the primary function of making a solid-fluid mixture behave as a fluid, this technology has the potential to reduce the harmful gas emissions from industries without compromising on the efficiency of results like combustion, catalytic cracking, and other chemical processes. Therefore, it is important to develop computational models to predict the flow characteristics inside the fluidized bed for further development of this potential sustainable technology that can replace the existing ones.

Similarly, blood plasma extraction plays a big part in the medical industry as the need for fresh blood and plasma is always in huge demand. The constituents in plasma are important in regulating cell function and maintaining homeostasis. Due to the immobility of the existing plasma extraction devices, the plasma extraction process becomes complex. Deployment of the Micro-plasma extractors into the market can immensely speed the process of plasma extraction without much complexity. Hence, detailed research into modelling of such dispersed flows in microchannels can immensely aid in the advancements of such technologies.

# CHAPTER 2
# OBJECTIVE OF WORK

- **Scientific Objective – I**

To identify the most reliable drag correlation for computational modelling of Dispersed Multiphase flows.

- **Scientific Objective – II**

To see if a drag correlation performs equally well across two very different and distinct domains dealing with the same type of flow.

- **Scientific Objective – III**

To identify the miniscule parameters in a Multiphase study that can have significant impact on the end result.

- **Scientific Objective – IV**

To study the efficiency of Plasma extraction from a blood sample in a novel Backward facing step Microchannel design using a Single-phase analysis.

- **Scientific Objective – V**

To understand the accuracy of Multiphase models in simulating a Fluidized Bed case by comparing with the experimental results obtained for the same.

# CHAPTER 3
# METHODOLOGY

The present study is primarily classified into two categories on the basis of industrial applications:

1) Medical Sector

2) Petroleum Sector

but deals with a common ground between the two, which is the Multiphase flows. Individual methodologies adopted to simulate cases related to both the sectors in discusses in this section of the project report.

## 3.1 PETROLEUM SECTOR – FLUIDIZED BED

The burgeoning research on Fluidized Beds due to its benefits over other industrial technologies is briefly discussed in the section 1.3. For further advancement and proliferation of this technology, research into Computational models that are capable of predicting the flow structure inside the Fluidized Bed accurately is of key interest. Realizing the importance of computational studies, the background research for this project began with a thorough understanding of the physics behind the computational models developed for Multiphase flows.

The geometry and boundaries of the 2D fluidized bed used for this study are shown in Figure 1. Figure 2, adopted from [2] shows the parts of a Fluidized bed and the lateral locations where the particle velocities are measured for comparison with the experimental data produced by National Energy Technology Laboratory (NETL). The corresponding dimensions and few parameters like the superficial gas velocity at the inlet, the initial packing fraction of the dispersed phase (particles) are mentioned in Table 1. An initial packing fraction of 0.58 means that 58% of the static bed is occupied with the dispersed phase (particles) and the remaining 42% with the continuous phase (liquid). In this study of the two-phase flow inside the fluidized bed for various drag correlations, the *twoPhaseEulerFoam* solver is used.

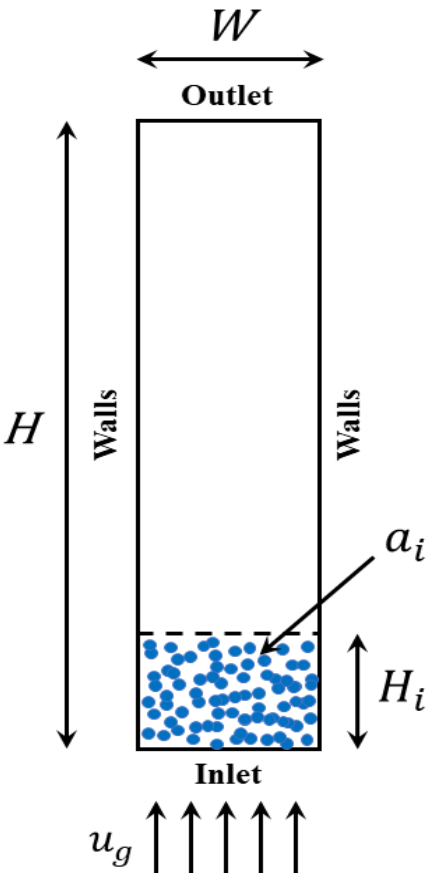


Figure 1: Fluidized bed model

| Parameters | Value |
|---|---|
| Superficial Gas Velocities ($u_g$) | 2.19 m/s & 3.28 m/s |
| Minimum Fluidization Velocity | 1.03 m/s |
| Static Bed Height ($H_i$) | 0.173 m |
| Initial phase fraction ($\alpha_i$) | 0.58 |
| Gas density ($\rho_g$) | 1.204 kg/m$^3$ |
| Particle diameter ($d_p$) | 3256 μm |
| Particle density ($\rho_p$) | 1131 kg/m$^3$ |
| Specularity Coefficient ($\Phi$) | 0.125 & 0.05 |

Table 1: Dimensions and parameters used in this study

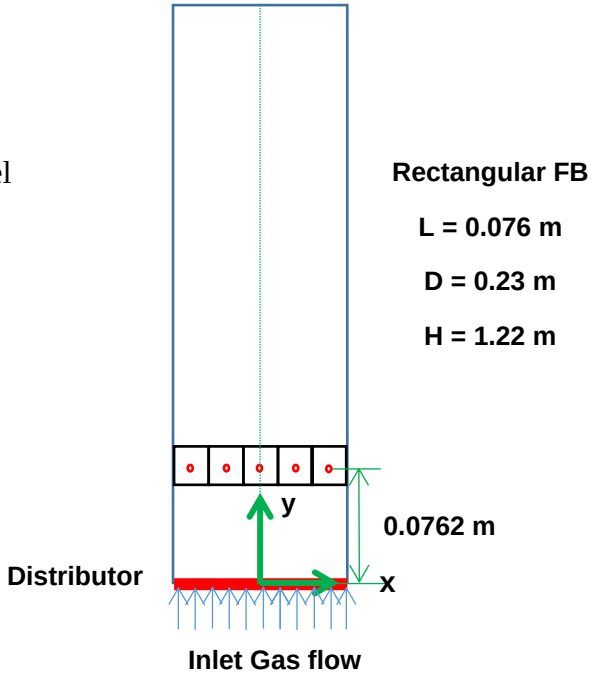


Figure 2: Fluidized bed with marked lateral locations for particle velocity measurement [1]

Like any fluid flow problem, Multiphase flows are also governed by a set of fundamental equations called the governing equations. They are discussed in detail in the sub-section 3.1.1 followed by a brief overview of the drag correlations implemented in this study.

### 3.1.1 Governing Equations

Multiphase flows are numerically modelled using different approaches such as:

1. Direct Numerical Simulation (DNS)
2. Eulerian – Langrangian approach
3. Eulerian – Eulerian approach

Eulerian – Eulerian approach is chosen for this study due to its relative computational inexpensiveness when compared to other approaches. This approach is further classified based on the phase morphology into separated and dispersed systems [1]. The fluidized bed being a dispersed system, multi-fluid modelling is used where both phases are treated as interacting and interpenetrating continua, therefore, share the same basic continuity and momentum equations for each phase individually as shown in Eqs. (1), (2), and (4). For the solid phase, the Kinetic Theory of Granular Flow (KTGF) [3] was adopted for closure which considers the conservation of Solid Fluctuation Energy. KTFG approach is an extension to the classical kinetic theory of gases to dense particulate flows, where the fluctuation energy is described with the help of granular temperature ($\theta$).

Three important assumptions made in this study for simplification are:

1. Both solid and liquid phases are isothermal.
2. There is no interphase mass transfer between both phases.
3. Solid particles are of pure spherical configuration with a mean diameter and density.

- Conservation of Mass (k = f for fluid phase, k = s for solid phase)

$$\frac{\partial}{\partial t}(\alpha_k \rho_k) + \frac{\partial}{\partial x}(\alpha_k \rho_k \boldsymbol{u}_k) = 0 \tag{1}$$

- Conservation of Momentum (fluid phase)

$$\frac{\partial}{\partial t}(\alpha_f \rho_f \boldsymbol{u}_f) + \nabla \cdot (\alpha_f \rho_f \boldsymbol{u}_f \boldsymbol{u}_f) = \alpha_f \nabla \cdot \bar{\boldsymbol{\tau}}_f + \alpha_f \rho_f \boldsymbol{g} - \alpha_f \nabla p - \boldsymbol{F}_{df} - \boldsymbol{F}_{vm} - \boldsymbol{F}_{lf} \tag{2}$$

$\boldsymbol{F}_{df}$, $\boldsymbol{F}_{vm,}$ $\boldsymbol{F}_{lf}$ is the drag force, virtual mass force, and lift force respectively in equations (2) and (4). Since drag force contributes predominantly to the momentum exchange between the fluid and solid phases, it is given more importance in this study.

The stress tensor of the liquid phase from Eq. (2) is expanded in Eq. (3)

$$\bar{\boldsymbol{\tau}}_f = \mu_f \left[\nabla \boldsymbol{u}_f + \left(\nabla \boldsymbol{u}_f\right)^T\right] - \frac{2}{3}\mu_f \left(\nabla \cdot \boldsymbol{u}_f\right)\bar{\boldsymbol{I}} \tag{3}$$

where $\mu_f$is the combined turbulent and laminar viscosity for the fluid phase. Further, $k{-}\varepsilon$ turbulence model is used in the study for the fluid phase.

- Conservation of Momentum (solid phase)

$$\frac{\partial}{\partial t}(\alpha_s \rho_s \boldsymbol{u}_s) + \nabla \cdot (\alpha_s \rho_s \boldsymbol{u}_s \boldsymbol{u}_s) = -\alpha_s \nabla p - \nabla p_s + \nabla \cdot \bar{\boldsymbol{\tau}}_s + \alpha_s \rho_s \mathbf{g} + \boldsymbol{F}_{df} + F_{vm} + F_{lf} \tag{4}$$

The solid phase stress tensor is expressed in terms of bulk solid viscosity $\xi_s$, and shear solid viscosity $\mu_s$ in Eq. (5)

$$\bar{\boldsymbol{\tau}}_s = \mu_s \left\{[\nabla \boldsymbol{u}_s + (\nabla \boldsymbol{u}_s)^T] - \frac{2}{3}(\nabla \cdot \boldsymbol{u}_s)\bar{\boldsymbol{I}}\right\} + \xi_s \nabla \cdot \boldsymbol{u}_s \bar{\boldsymbol{I}} \tag{5}$$

- Conservation of Solid Fluctuation Energy

$$\frac{3}{2}\left[\frac{\partial}{\partial t}(\alpha_s \rho_s \theta) + \nabla \cdot (\alpha_s \rho_s \theta)\boldsymbol{u}_s\right] = \left(-\nabla p_s \bar{\boldsymbol{I}} + \bar{\boldsymbol{\tau}}_s\right) : \nabla \boldsymbol{u}_s + \nabla \cdot (k_s \nabla \theta) - \gamma_s - 3\beta\theta + D_{l_s} \tag{6}$$

Granular temperature is used to measure the energy of fluctuating velocity of particles.

### 3.1.2 Drag correlations

Numerous drag correlations are available in the literature [1] that can model the mechanism of interphase momentum transfer majorly caused due to drag force between the phases. A thorough literature study was performed to identify such drag correlations that could model the flow for all packing fraction regimes, individually or as a combination of two. It is important for a drag correlation to accurately predict the flow at all packing fraction regimes because, the probability of a cell in a domain, especially at the interface, to overshoot the maximum packing fraction of the domain can never be neglected and must be taken into account. Also, the correlations adopted must be applicable for a multi-particle system to consider the effect of other particle's presence. Upon considering such fundamental factors, three drag correlations were chosen to model the two-phase flow inside a fluidized bed.

a) Gidaspow-Ergun-Wen-Yu:

This is a combination of the Ergun drag correlation applicable for dense systems and the Wen Yu correlation that can model a dilute flow where viscous forces are dominant, accurately.

This correlation uses the Ergun equation, Eq. (7), for $\alpha_p \geq 0.2$ and the Wen–Yu equation, Eq. (8) for $\alpha_p \leq 0.2$, where K is defined as the drag function for each correlation. Drag force in the Ergun correlation is calculated based on pressure drop per unit length, Eq. (9), unlike the Wen Yu correlation that considers the drag coefficient on a single particle, Eq. (10).

$$K = 150\frac{\mu_g}{d_p}\frac{\alpha_p^2}{\left(1-\alpha_p\right)^2} + 1.75\frac{\rho_g U_r}{d_p}\frac{\alpha_p^2}{\left(1-\alpha_p\right)^2} \tag{7}$$

$$K = \frac{3}{4d_p}C_{Ds}\alpha_p\left(1-\alpha_p\right)\rho_g U_r\left(1-\alpha_p\right)^{-2.65} \tag{8}$$

$$\frac{\Delta p}{L} = 150\frac{\mu_g U_r}{d_p g}\frac{\alpha_p^2}{\left(1-\alpha_p\right)^3} + 1.75\frac{\rho_g U_r^2}{d_p g}\frac{\alpha_p}{\left(1-\alpha_p\right)^3} \tag{9}$$

$$C_{Ds} = \begin{cases} \frac{24}{\mathrm{Re}}\left(1+0.15\mathrm{Re}^{0.687}\right), & \mathrm{Re} \leq 1000 \\ 0.44, & \mathrm{Re} > 1000 \end{cases} \tag{10}$$

b) Gidaspow-Schiller-Naumann:

This drag correlation is capable of calculating the drag in a multi-particle system, unlike the Schiller-Naumann correlation which is restricted to a single particle system only. The drag function for this correlation is defined in Eq. (11). Schiller-Naumann drag coefficient, Eq. (10), is used by replacing the Re with $(1-\alpha_p)\mathrm{Re}$, as shown in Eq. (12) below.

$$K = \frac{3}{4d_p}C_{Ds}\alpha_p\left(1-\alpha_p\right)\rho_l U_r\left(1-\alpha_p\right)^{-2.65} \tag{11}$$

$$C_{Ds} = \begin{cases} \frac{24}{\left(1-\alpha_p\right)\mathrm{Re}}\left(1+0.15\left((1-\alpha_p)\mathrm{Re}\right)^{0.687}\right), & \mathrm{Re} \leq 1000 \\ 0.44, & \mathrm{Re} > 1000 \end{cases} \tag{12}$$

c) Syamlal O'Brien

This drag correlation is based on the primary assumption that the Archimedes number remains the same for terminal settling velocity for both single and multi-particle systems. It uses the expression, Eq. (13), to relate the settling velocity and the void fraction, where $\mathrm{Re}_s$ is the Reynolds number for a single particle and $V_r$, the ratio of terminal settling velocity in a multi-particle system to that of a single particle system.

$$\frac{V_r - A}{B - V_r} = 0.06\mathrm{Re}_s \tag{13}$$

$$V_r = 0.5\left(A - 0.06\mathrm{Re} + \sqrt{(0.06\mathrm{Re})^2 + 0.12\mathrm{Re}\,(2B - A) + A^2}\right) \tag{14}$$

$$A = \left(1 - \alpha_p\right)^{4.14} \tag{15}$$

$$B = \begin{cases} \mathbf{C}_1\left(1 - \alpha_p\right)^{1.28}, \alpha_p \geq 0.15 \\ \left(1 - \alpha_p\right)^{\mathbf{C}_2}, \alpha_p < 0.15 \end{cases} \tag{16}$$

Eq. (14), (15), and (16) are obtained by solving Eq. (13) after replacing $\mathrm{Re}_s$ with $\mathrm{Re}/V_r$. Drag coefficient proposed by Dallavalle, Eq. (17), is used here to obtain the final drag function in Eq. (18), where $\mathbf{U}_r$ is the relative velocity interstitial velocity, $\mathbf{U}_g - \mathbf{U}_p$.

$$C_{Ds} = \left(0.63 + \frac{4.8}{\sqrt{\mathrm{Re}_s}}\right)^2 \tag{17}$$

$$K = \frac{3\alpha_p\left(1 - \alpha_p\right)\rho_g}{4V_r^2 d_p}\left(0.63 + 4.8\sqrt{\left(\frac{V_r}{\mathrm{Re}}\right)}\right)^2 |\mathbf{U}_r| \tag{18}$$

The coefficients $\mathbf{C}_1$ and $\mathbf{C}_2$ in Eq. (16) are unique to a problem statement and depend on the parameters like Archimedes number, minimum fluidization velocity, and other physics properties of the individual phases. In our case, $\mathbf{C}_1 = 0.88$ and $\mathbf{C}_2 = 2.04$. Existing Syamlal O'Brien drag correlation was tuned with the new coefficients by creating a new drag model with the name *newSyamlalObrien.*

### 3.1.3 Johnson & Jackson model

Unlike the fluid flow where a *noSlip* condition is applied to the walls, particles in a granular flow fluctuate between the two extremes of sticking to the wall and sliding on it. For the same reason, Johnson and Jackson developed boundary conditions [7] that relate the solid phase velocity with that of its granular temperature as shown in Eqs. (19) and (20).

$$\mu_s \frac{\partial u_s}{\partial x} = -\frac{\pi \phi_s \rho_s \alpha_s g_0 \sqrt{\theta_s}}{2\sqrt{3}\alpha_s^{max}} u_s \tag{19}$$

$$\kappa_s \frac{\partial \theta_s}{\partial x} = -\frac{\pi \phi_s u_s^2 \rho_s \alpha_s g_0 \sqrt{\theta_s}}{2\sqrt{3}\alpha_s^{max}} - \frac{\pi\sqrt{3}\rho_s \alpha_s g_0 (1 - e_W^2)\sqrt{\theta_s}}{4\alpha_s^{max}} \theta_s \tag{20}$$

$u_s$ and $\kappa_s$ are viscosity and conductivity of solid phase, $\phi_s$ and $e_W^1$ are specularity coefficient and particle-wall coefficient of restitution. The granular temperature is made non-zero at t=0 in all the cells by defining a parameter called *referenceLevel* = 1e-4 in *Theta.particles* script file to avoid invalid mathematical operations. Table 2 contains the specularity coefficient and coefficient of restitution for particle – wall interactions considered in this case study.

### 3.1.4 Effect of Specularity coefficient

Specularity coefficient ($\phi_s$) is defined as the = fraction of particle tangential momentum transferred to wall through collisions. It is an indicative of the wall roughness. This is affected by the superficial gas velocity and the particle size.

$\phi_s$ = 1 ⇒ Zero tangential velocity, maximum hindrance

$\phi_s = 0$ ⇒ Free slip along the wall, minimum hindrance

In our problem, the specularity coefficient was considered as 0.05 for 3.28 m/s gas velocity [5] and 0.125 for 2.19 m/s gas velocity which yielded more accurate results

### 3.1.5 Simulation procedure

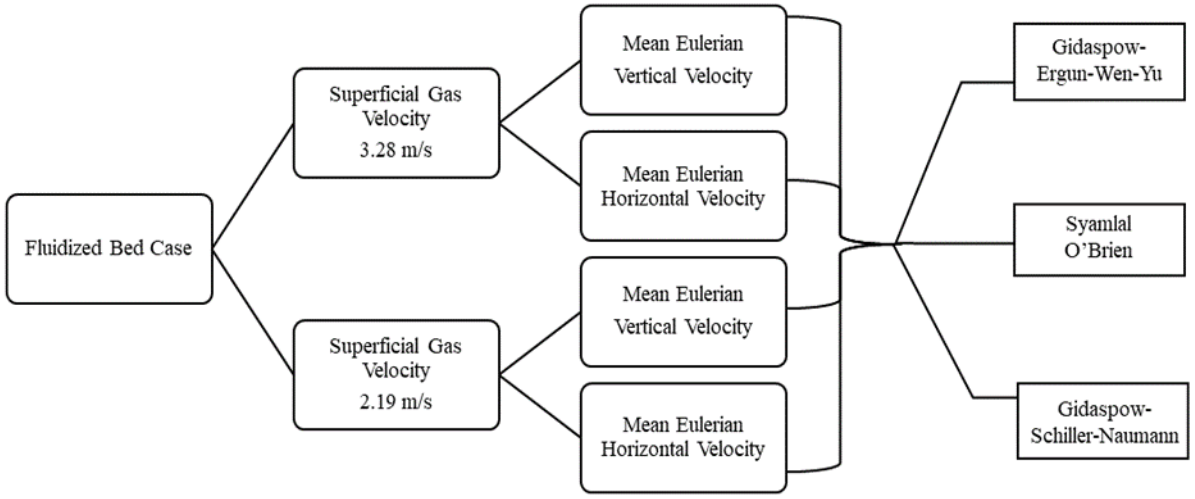


Figure 3: Classification of the Fluidized Bed case

The set of cases that are to be simulated in OpenFOAM for this study is shown in the form of a classification chart in Figure 3. The fluidized bed is a standard case study, readily existing in the tutorial directory of OpenFOAM under *twoPhaseEulerFoam* solver. Initially, the tutorial case file has to be copied into the run directory which is our working directory. The 0/constant/system folders containing various script files for defining the initial and boundary conditions, physical and phase properties, simulation control, and a few more are to be modified according to our requirements. Further, case files are accessed using the terminal to run the simulation using multiple commands.

After the simulation is complete, post-processing of the results is performed in ParaView, an open-source visualization software. Particle velocity data at every timestamp is extracted by plotting the data over time for the required lateral location. The data obtained for all the cases are consolidated in one spreadsheet to plot the velocity distribution against lateral location for all three drag correlations. The results are compared with the experimental data generated by NETL [4] for validation and understanding the reliability of a drag correlation in modelling a dispersed multiphase simulation accurately.

### 3.1.6 Geometry and Mesh

The computational domain used to simulate the problem of the fluidized bed is shown in Figure 3. A 2D domain is chosen to make the multiphase simulation computationally less expensive. The dimensions of the domain are already marked in Figure 1. It is made sure that the edge dimensions of an element are larger than the diameter of the particle for the averaged Navier Stokes to be valid. blockMesh utility is used for geometry and hexahedral mesh generation.

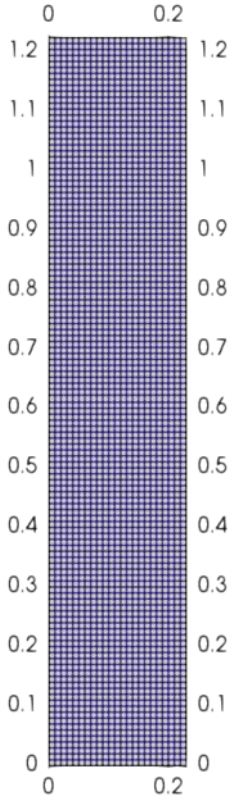


| Direction | Number of divisions |
|---|---|
| X - axis | 23 |
| Y - axis | 122 |
| Z - axis | 1 |

Table 2: Division of domain along the coordinate axis

Figure 4: 2D view of the computational domain

### 3.1.7 Initial and Boundary Conditions

The initial and boundary conditions of the field variables defined in Table 4-7 are of prime importance in defining how the flow develops inside the physical domain. The reason for defining *interstitialInletVelocity* condition over a *fixedValue* boundary condition for *U.air* is because of the transient nature of the simulation where the packing fraction of the phases keep changing with time. Similarly, *pressureInletOutletVelocity* is defined at the outlet for the flow to switch between *zeroGradient* and *fixedValue* conditions during the occurrence of a reverse flow.

| Boundary | U.air (m/s) | U. particles (m/s) |
|---|---|---|
| Inlet | interstitialInletVelocity<br>(0 2.19 0) & alpha.air | fixedValue<br>(0 0 0) |
| Outlet | pressureInletOutletVelocity<br>phi.air | fixedValue<br>(0 0 0) |
| Walls | noSlip | JohnsonJacksonParticleSlip |

Table 3: Velocity boundary conditions

| Boundary | alpha | P_rgh | Theta |
|---|---|---|---|
| Inlet | zeroGradient | fixedFluxPressure | fixedValue |
| Outlet | zeroGradient | prghPressure<br>p = 101325 Pa | zeroGradient |
| Walls | zeroGradient | fixedFluxPressure | JohnsonJacksonParticleTheta |

Table 4: Miscellaneous boundary conditions

| Boundary | k.air | epsilon.air | nut.air |
|---|---|---|---|
| Inlet | fixedValue | fixedValue | calculated |
| Outlet | inletOutlet | inletOutlet | calculated |
| Walls | kqRWallFunction | epsilonWallFunction | nutkWallFunction |

Table 5: Turbulence boundary conditions

| Boundary | T.air (m/s) | T. particles (m/s) |
|---|---|---|
| Inlet | zeroGradient | zeroGradient |
| Outlet | inletOutlet type | inletOutlet type |
| Walls | zeroGradient | zeroGradient |

Table 6: Temperature boundary conditions

In a granular flow case, the particles neither stick to the wall nor slip freely on it. They oscillate between both these conditions and for the same reason, *JohnsonJacksonParticleSlip* condition is applied for the walls of both *U. particles* and *Theta.particles* field variables.

*frontAndBackPlanes* boundary is common for all field variables in the 0 folder. Since it is a 2D simulation problem, *empty* condition is defined for the boundary.
At t = 0, the column is filled with particles whose static bed height is 0.173m, as shown in Figure 1. Also, the initial packing fraction of the particles is 0.58 within the static bed and 0 in the remaining column volume. These non-uniform initial conditions are defined in the *setFields* utility of the *system* folder.

### 3.1.8 Solver Details

The *twoPhaseEulerFoam* is a Eulerian–Eulerian multiphase solver readily available in the open-source CFD toolbox, OpenFOAM. It is used for a system of 2 non-reacting compressible fluid phases, where one phase is always dispersed, making it a reliable solver for gas-solid fluidized systems and many other applications. It uses the Finite Volume Method (FVM) to solve cell-centred and phase-averaged governing equations. Each of the phases are treated as a continuum in this approach.

### 3.2 MEDICAL SECTOR – PLASMA EXTRACTION MICROCHANNELS

A Backward-Facing Step is a widely used geometry to induce flow separation and recirculation caused by sudden expansion of the configuration. Its implementation ranges from internal to external flows. In our case of an internal blood flow, three designs of BFS Microchannels Figure 5,6, and 7 from [4] are used to evaluate the efficiency of plasma extraction in each design and choose the one with the maximum extraction efficiency to conduct the Multiphase blood simulations. The methodology followed to simulate the single-phase and Multiphase flow inside the microchannels is discussed in sections 3.2.1 to 3.2.4

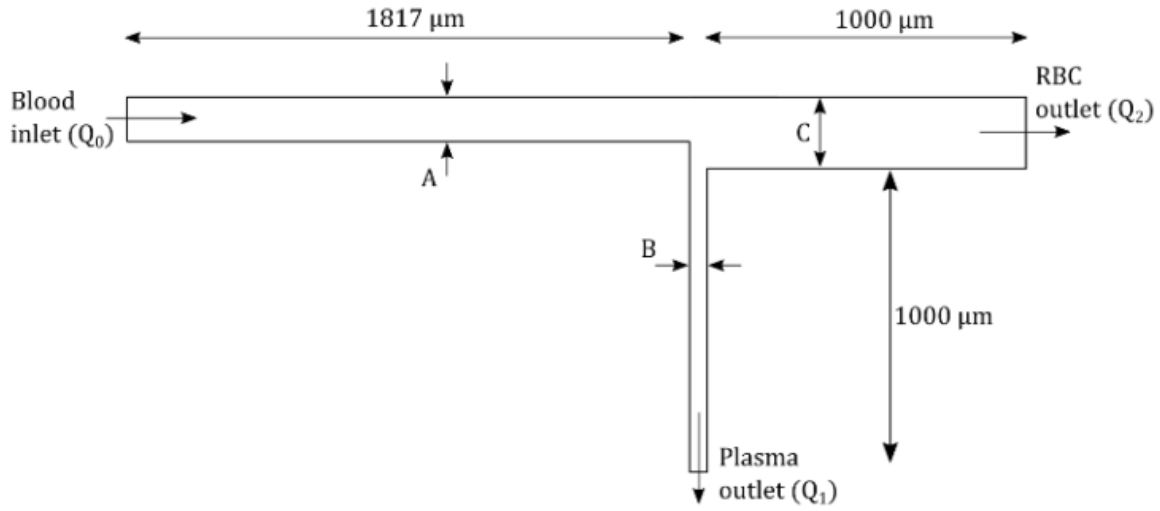


Figure 5: Type I Microchannel with dimensions

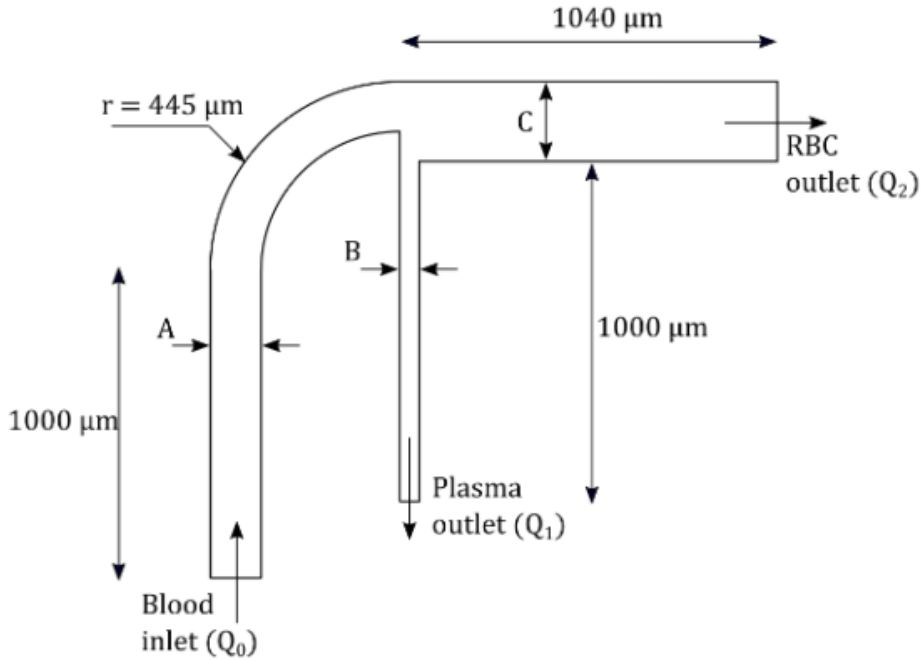


Figure 6: Type II Microchannel with dimensions

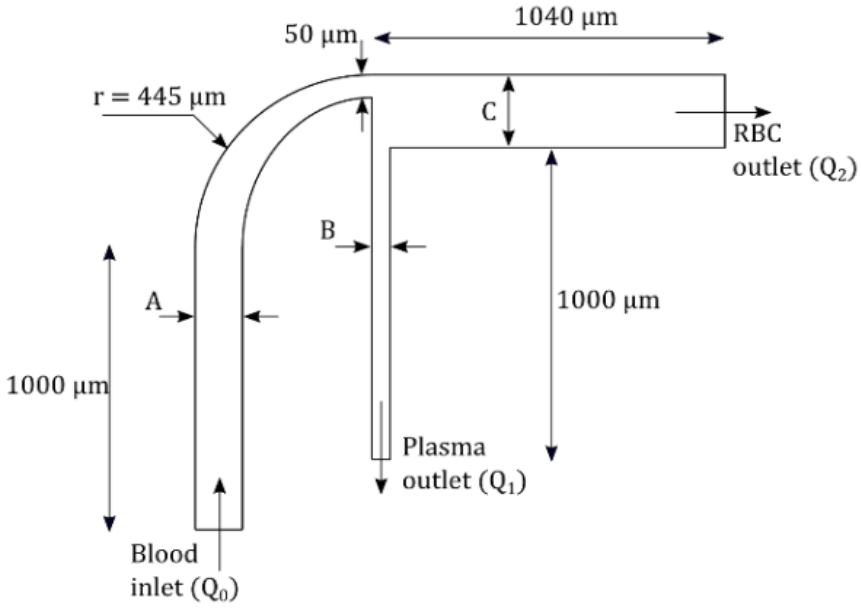


Figure 7: Type III Microchannel with dimensions

**Single-phase Study**

### 3.2.1 Governing Equations

- Conservation of Mass

$$\nabla \cdot \vec{u} = 0 \tag{20}$$

- Conservation of Momentum

$$\nabla \cdot (\vec{u} \otimes \vec{u}) - \nabla \cdot \mathbf{T} = -\nabla p + \mathbf{S}_u \tag{21}$$

In the above Eqs. (20) and (21), $\vec{u}$ is the velocity, $p$ is the kinematic pressure, **T** is the stress tensor and $\mathbf{S}_u$ is the momentum source.

Water is considered as the single-phase fluid in this simulation with the properties as mentioned in Table 8.

| Parameters | Value |
|---|---|
| Density | 997 kg/m$^3$ |
| Viscosity | 8.55×10-4 kg/m-s |
| Reynolds Number | 5 |



Table 7: Single-phase study parameters

### 3.2.2 Geometry and Mesh

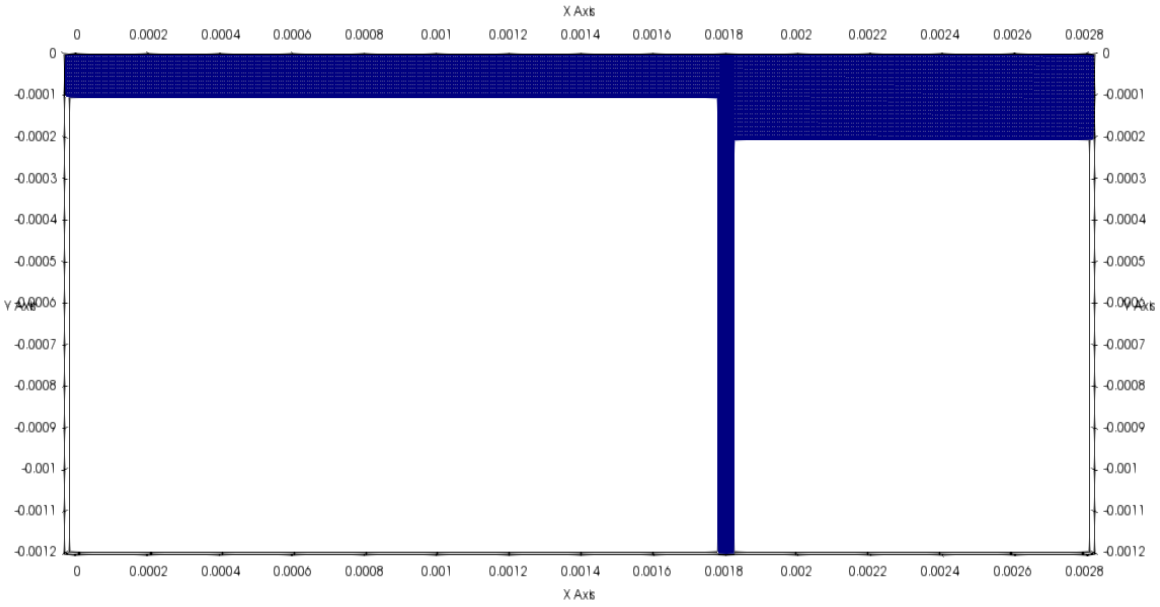


Figure 8: Type I Microchannel Mesh (4,84,021 elements)

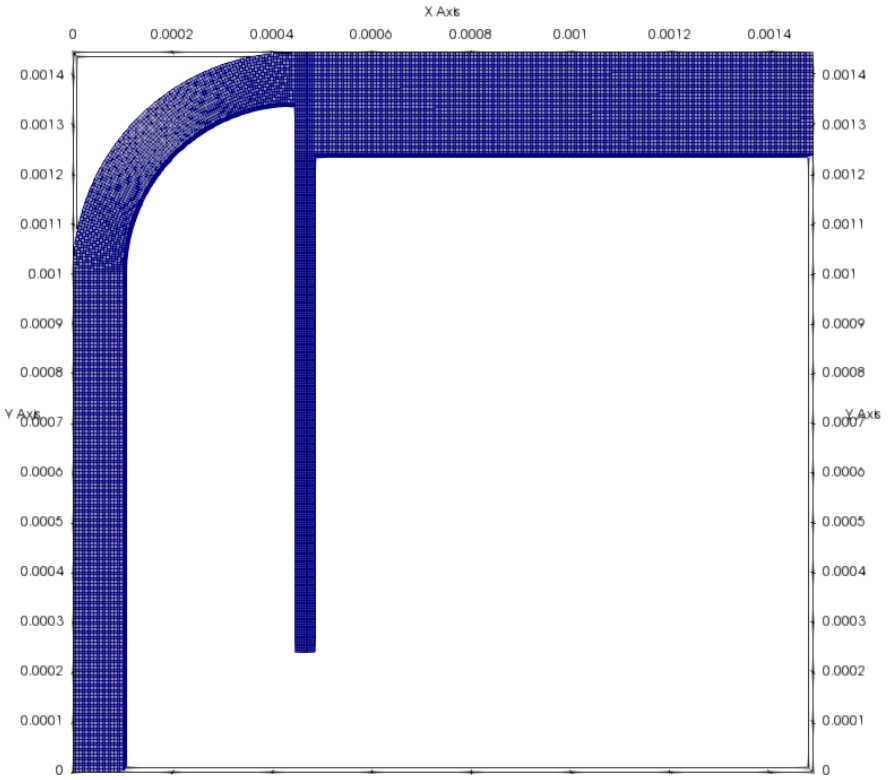


Figure 9: Type II Microchannel mesh (4,72,021 elements)

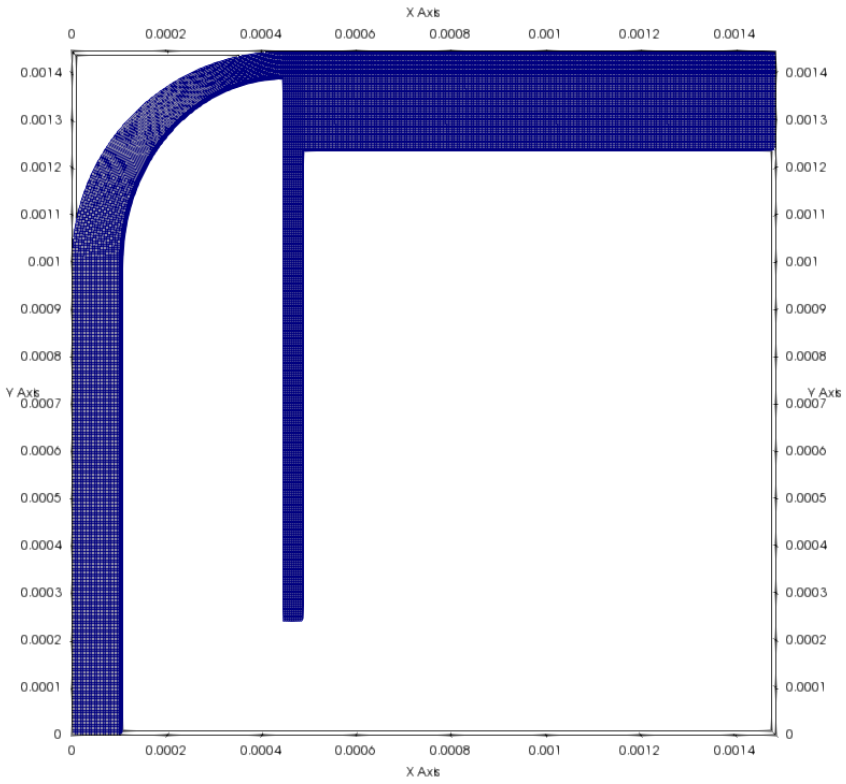


Figure 10: Type III Microchannel mesh (5,00,714 elements)

### 3.2.3 Boundary conditions

| **Boundary** | $\boldsymbol{p}(\mathrm{m}^2/s^2)$ | **u** $(\mathrm{m}/\mathrm{s})$ |
|---|---|---|
| Inlet | zeroGradient | 0.075 |
| Outlet | fixedValue | zeroGradient |
| Walls | zeroGradient | noSlip |

Table 8: Single-phase study Boundary conditions

### 3.2.4 Solver Details

To analyse the steady state laminar flow, which is the case of a single-phase flow in a microchannel, *simpleFoam* solver is used. *simpleFoam* is a steady-state solver for incompressible, laminar, and turbulent flow. The solver utilizes "Semi-Implicit Method for Pressure-Linked Equations" (SIMPLE) algorithm. Finite volume method and three-dimensional structured grid are used to solve the governing equations for the steady, incompressible and laminar flow in this problem.

# Multiphase Study

### 3.2.5 Governing equations

- Conservation of Mass

$$\frac{\partial}{\partial t}(\alpha_k \rho_k) + \frac{\partial}{\partial x}(\alpha_k \rho_k \boldsymbol{u}_k) = 0 \tag{22}$$

- Conservation of Momentum

$$\frac{\partial}{\partial t}(\alpha_k \rho_k \boldsymbol{u}_k) + \nabla \cdot (\alpha_k \rho_k \boldsymbol{u}_k \boldsymbol{u}_k) = \alpha_k \nabla \cdot \bar{\boldsymbol{\tau}}_k + \alpha_k \rho_k \boldsymbol{g} - \alpha_k \nabla p - \boldsymbol{F}_{df} - \boldsymbol{F}_{vm} - \boldsymbol{F}_{lf} \tag{23}$$

Based on the conclusion from the Fluidized bed study in section 3.1, Syamlal O'Brien drag correlation is implemented in the study to investigate its effectiveness in modelling a Multiphase Blood flow. The density and kinematic viscosity of plasma were taken to be 1025 kg/m3 and 1.2×10-6 m2 /s respectively, while for RBCs, the same were considered to be 1110 kg/m3 and 5×10-6 m2 /s respectively. An additional interface sharpening methodology is employed in multiphaseEulerFoam.

### 3.2.6 Geometry and Mesh

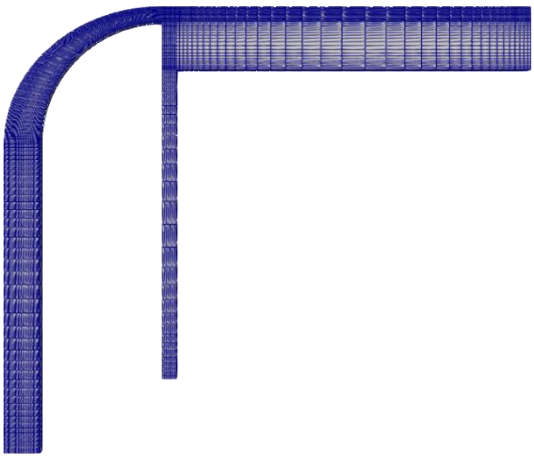

The geometry from the single-phase simulation is retained for this study. However, the inlet is split in the ratio 4:1 for the pure plasma to through the larger section and the mixed fluid to enter through the smaller one. A two-dimensional study was conducted and the number of elements were kept low keeping in mind the computational time and expensiveness of a Multiphase simulation.

### 3.2.7 Boundary Conditions

| **Boundary** | $\boldsymbol{p}(\mathrm{m}^2/s^2)$ | **u** $(\mathrm{m/s})$ | $\mathbf{k}_{plasma}$ | $\mathbf{K}_{RBC}$ |
|---|---|---|---|---|
| Mixed Inlet | zeroGradient | 0.075 | 0.5 | 0.5 |
| Plasma Inlet | zeroGradient | 0.075 | 1 | 0 |
| Outlets | fixedValue | zeroGradient | zeroGradient | zeroGradient |
| Walls | zeroGradient | noSlip | zeroGradient | zeroGradient |

Table 9: Multiphase study Boundary conditions

### 3.2.8 Solver Details

The *multiPhaseEulerFoam* is a Eulerian–Eulerian multiphase solver readily available in the open-source CFD toolbox, OpenFOAM. It is used for a system of many non-reacting compressible fluid phases. It uses the Finite Volume Method (FVM) to solve cell-centred and phase-averaged governing equations. Each of the phases are treated as a continuum in this approach.

# CHAPTER 4
# RESULTS AND DISCUSSION

## 4.1 FLUIDIZED BED – MULTIPHASE STUDY

Post-processing of the results was carried out in ParaView and Excel. Particle velocity at different lateral locations was obtained by plotting the entire transient simulation over time for each lateral location to extract the velocity data at every time step for all 50 seconds. The extracted data was time-averaged in the time interval after a bubbling fluidization flow regime is established which is sustained till the end of the simulation. Figure 11 shows the contours for particle phase fraction at various time stamps for the Syamlal O'Brien drag correlation for the superficial gas velocity of 2.19 m/s.

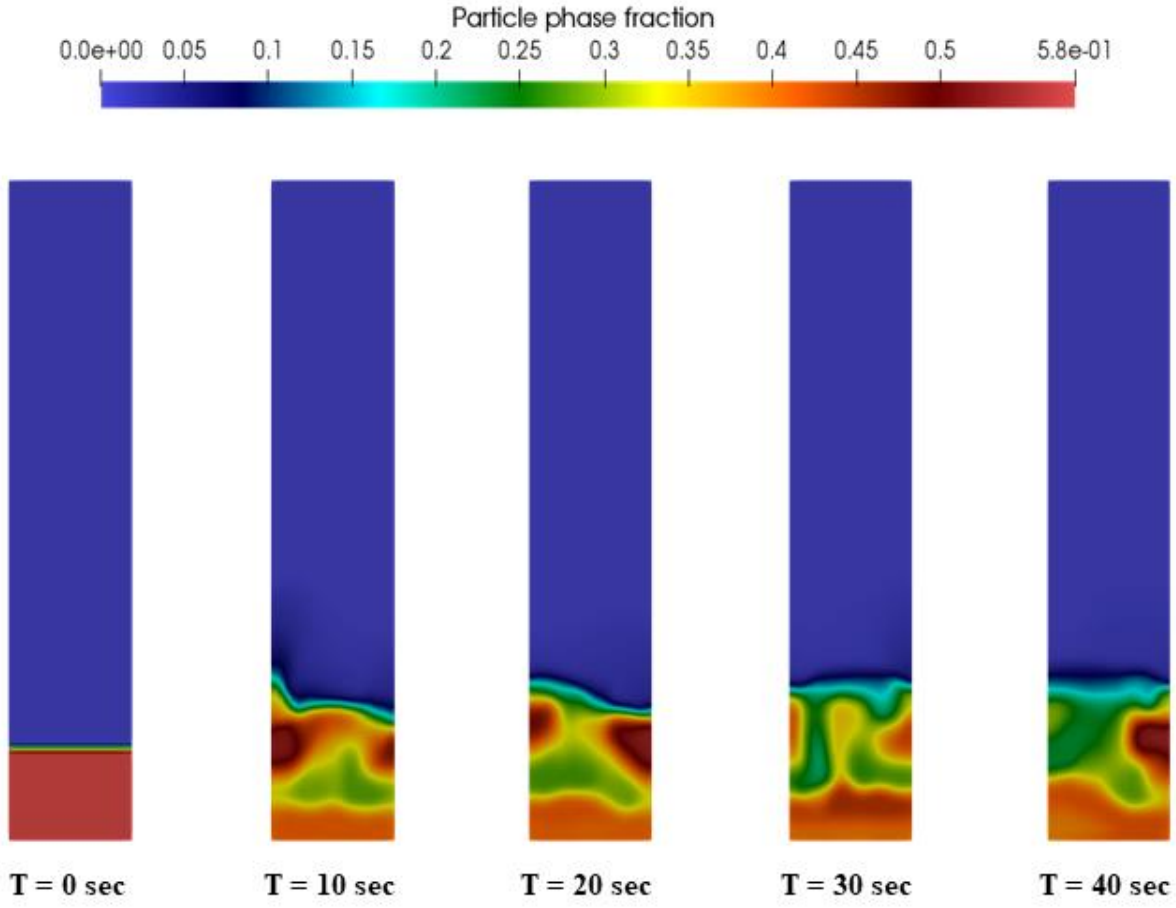


Figure 11: Contours of particle phase fraction ($\alpha_p$) at five different timestamps

### 4.1.1 Result 1: Mean Eulerian Vertical Velocity Distribution (for $U_g$= 2.19 m/s)

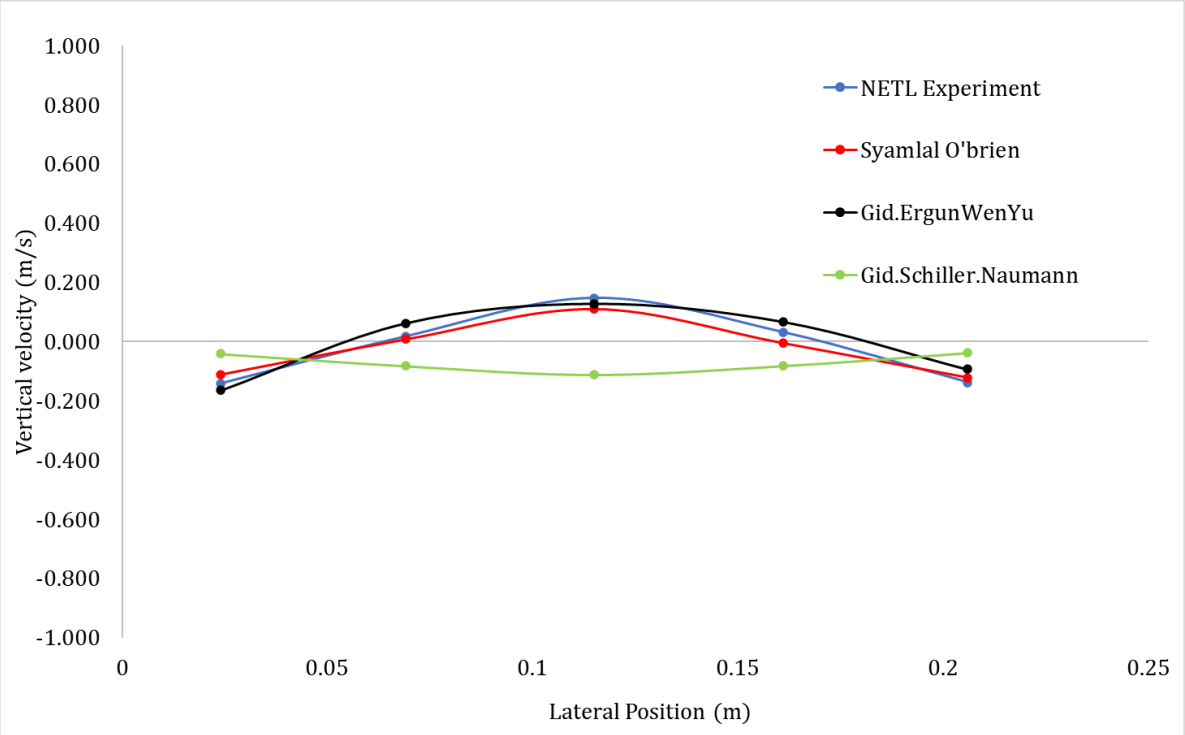


Figure 12: Vertical velocity vs Lateral position plot for various drag correlations ($\mathbf{U}_g$= 2.19 m/s)

| X | NETL Experiment | Syamlal O'Brien | Rel. Error wrt Expt | GEW | Rel. Error wrt Expt | GSN | Rel. Error wrt Expt |
|---|---|---|---|---|---|---|---|
| 0.024 | -0.142 | -0.111 | 0.216 | -0.164 | 0.746 | -0.042 | 0.707 |
| 0.069 | 0.017 | 0.008 | 0.531 | 0.062 | 1.990 | -0.083 | 5.855 |
| 0.115 | 0.147 | 0.111 | 0.599 | 0.128 | 0.469 | -0.112 | 1.762 |
| 0.161 | 0.031 | -0.005 | 1.156 | 0.066 | 0.075 | -0.082 | 3.646 |
| 0.206 | -0.138 | -0.122 | 0.118 | -0.094 | 0.280 | -0.038 | 0.724 |

Table 10: Relative error in velocity measurements of drag models wrt. experimental results

The time-averaged axial velocity data of the particles at different lateral locations of the fluidized bed is plotted in fig. 3 for different drag correlations. Experimental data generated by NETL for the same is included for comparison with the CFD results. Syamlal O'Brien drag closure is more accurate in predicting the axial particle velocity at all the lateral locations, followed by GEW. The trend of experimental results is followed by both Syamlal O'Brien and GEW but not GSN. The time-averaged axial velocity is the highest at the central location for all correlations except GSN.

### 4.1.2 Result 2: Mean Eulerian Horizontal Velocity Distribution (for $U_g$= 2.19 m/s)

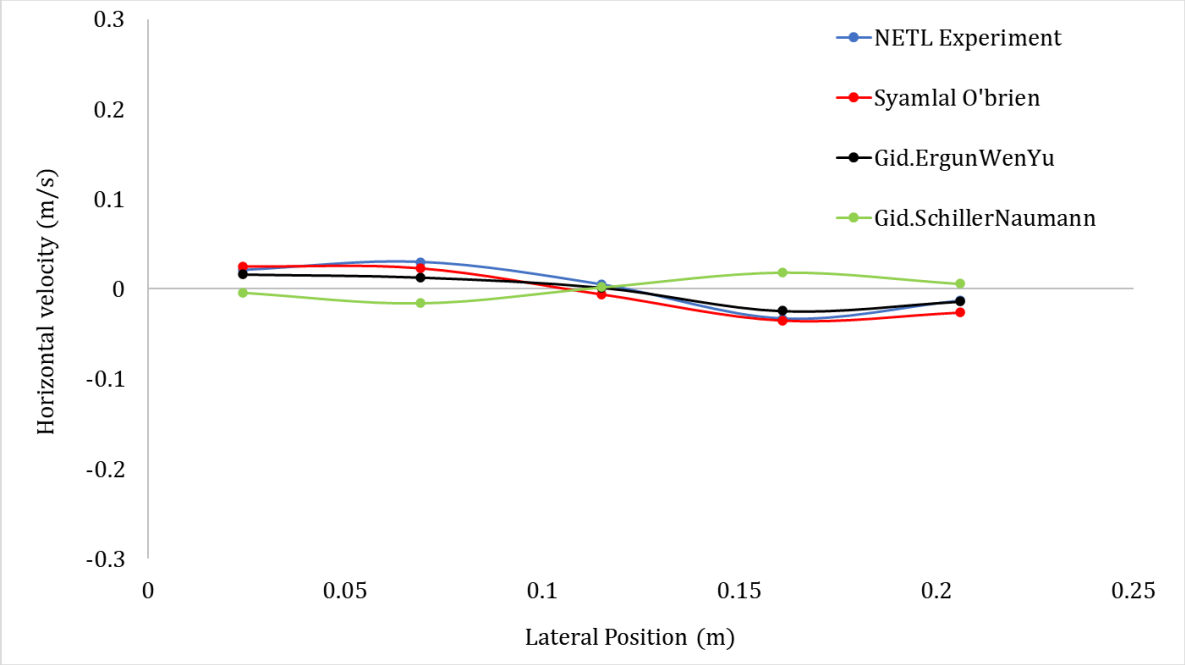


Figure 13: Horizontal velocity vs Lateral position plot for various drag correlations ($\mathbf{U}_g$= 2.19 m/s)

| X | NETL Experiment | Syamlal O'Brien | Rel. Error wrt Expt | GEW | Rel. Error wrt Expt | GSN | Rel. Error wrt Expt |
|---|---|---|---|---|---|---|---|
| 0.024 | 0.021 | 0.025 | 0.179 | 0.016 | 0.543 | -0.004 | 1.188 |
| 0.069 | 0.03 | 0.023 | 0.241 | 0.013 | 0.872 | -0.016 | 1.530 |
| 0.115 | 0.005 | -0.006 | 2.214 | 0.002 | 2.893 | 0.002 | 0.618 |
| 0.161 | -0.033 | -0.035 | 0.065 | -0.024 | 0.001 | 0.019 | 1.562 |
| 0.206 | -0.013 | -0.026 | 1.016 | -0.014 | 1.124 | 0.006 | 1.446 |

Table 11: Relative error in velocity measurements of drag models wrt. experimental results

The results obtained for horizontal velocity distribution, fig. 4, further strengthen our inference made from the axial velocity results about the accuracy of the Syamlal O'Brien correlation because of its overlapping with the experimental results. However, the GEW closure is nearly as accurate as of the Syamlal O'Brien closure for the first case. Similar to the axial velocity distribution, the GSN correlation fails to follow the trend of the experimental plot and overpredicts at most of the lateral positions.

### 4.1.3 Result 3: Mean Eulerian Vertical Velocity Distribution (for $U_g$= 3.28 m/s)

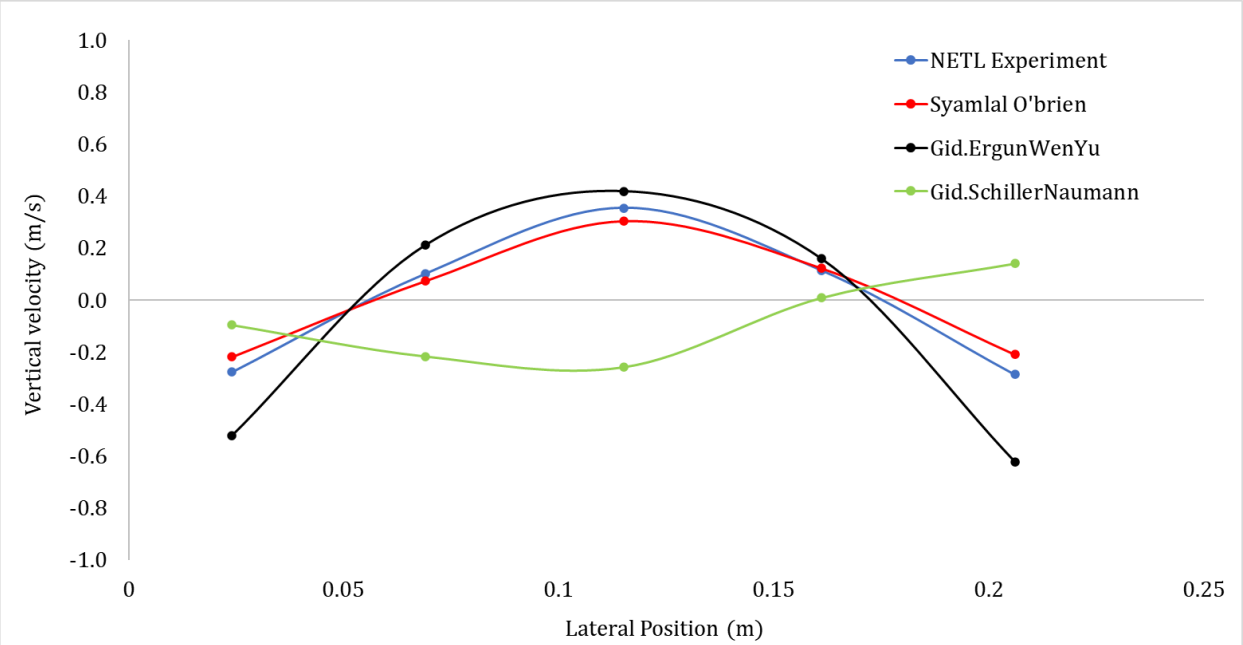


Figure 14: Vertical velocity vs Lateral position plot for various drag correlations ($U_g$= 3.28 m/s)

| X | NETL Experiment | Syamlal O'Brien | Rel. Error wrt Expt | GEW | Rel. Error wrt Expt | GSN | Rel. Error wrt Expt |
|---|---|---|---|---|---|---|---|
| 0.024 | -0.277 | -0.220 | 0.672 | -0.522 | 0.119 | -0.096 | 0.652 |
| 0.069 | 0.101 | 0.073 | 0.684 | 0.212 | 2.519 | -0.217 | 3.150 |
| 0.115 | 0.354 | 0.304 | 0.817 | 0.419 | 0.869 | -0.259 | 1.731 |
| 0.161 | 0.114 | 0.122 | 0.714 | 0.159 | 0.641 | 0.008 | 0.929 |
| 0.206 | -0.287 | -0.210 | 0.441 | -0.623 | 0.874 | 0.140 | 1.490 |

Table 12: Relative error in velocity measurements of drag models wrt. experimental results

Interesting behaviour was observed in the time-averaged vertical velocity distribution when the superficial gas velocity was increased from 2.19 m/s to 3.28 m/s as shown in Figure 14. Syamlal correlation again proved to be the accurate among others, though the relative error has slightly increased when compared to the 2.19 m/s vertical velocity distribution. The direction of velocity at the five lateral locations for both GEW and Syamlal correlation happens to be same as that of experimental observations which is not the case with GSN. Though GEW correlation has managed to successfully follow the trend of experimental results, the first and last lateral location values are highly deviating for GEW relative to Syamlal. Except for the first lateral location, the velocity direction was completely opposite to that of the experiment for GSN correlation.

### 4.1.4 Result 4: Mean Eulerian Horizontal Velocity Distribution (for $U_g$= 3.28 m/s)

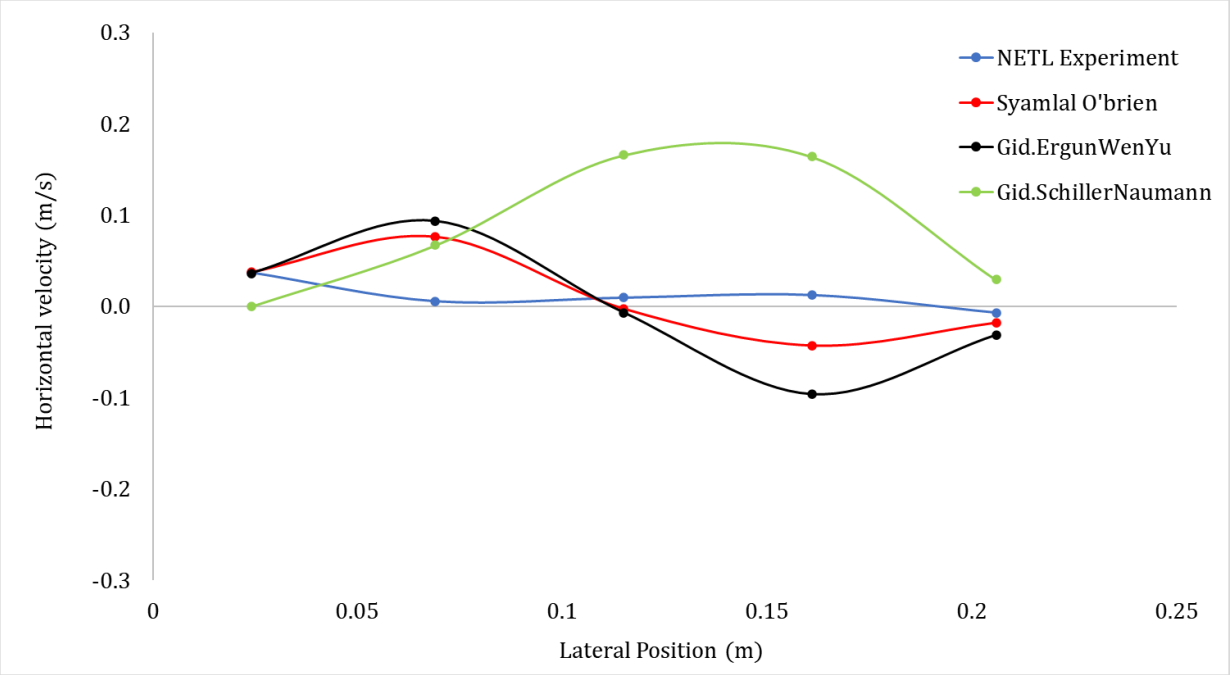


Figure 15: Horizontal velocity vs Lateral position plot for various drag correlations ($\mathbf{U}_g$= 3.28 m/s)

| X | NETL Experiment | Syamlal O'Brien | Rel. Error wrt Expt | GEW | Rel. Error wrt Expt | GSN | Rel. Error wrt Expt |
|---|---|---|---|---|---|---|---|
| 0.024 | 0.037 | 0.038 | 0.526 | 0.036 | 0.956 | 0.000 | 1.006 |
| 0.069 | 0.005 | 0.076 | 5.779 | 0.093 | 27.558 | 0.067 | 11.423 |
| 0.115 | 0.009 | -0.003 | 1.273 | -0.007 | 8.656 | 0.166 | 16.893 |
| 0.161 | 0.012 | -0.043 | 4.526 | -0.096 | 3.264 | 0.164 | 12.421 |
| 0.206 | -0.007 | -0.018 | 1.511 | -0.032 | 2.482 | 0.029 | 5.056 |

Table 13: Relative error in velocity measurements of drag models wrt. experimental results

At a particular lateral location, the CFD results obtained for the horizontal velocity, deviated more from the corresponding experimental values as depicted in Figure 15 when compared to the results that were obtained for the 2.19 m/s gas velocity. Surprisingly, the trend observed in experimental results was not followed by the drag correlations but, a similar trend was observed in the work of [5] for same values of gas velocity and similar drag correlations. Thus, the trend followed by Syamlal and GEW is what is expected out of a CFD simulation. However, GSN totally overpredicts the velocity at all lateral locations like it has performed for other cases as well.

### 4.1.5 Inferences from Fluidized Bed study

The first major inference that can be drawn from the results is that, out of the three drag correlations, the Gidaspow-Schiller-Naumann correlation predicted the particle velocity distributions poorly for both the cases of gas velocity. Despite being developed to account for the particle-particle interactions by including the voidage function, it was least accurate for both the velocity cases. This can be attributed to the fact that it was primarily developed for packed bed applications where the gas velocity is relatively low, restricting the flow regime to a fixed bed. The drastic increase in relative error as the gas velocity is raised from 2.19 m/s to 3.28 m/s for the GSN correlation reinforces our inference about the better performance of the GSN correlation at low fluid velocities and dilute particle concentrations.

Initially, vertical velocity profiles deviated the maximum from the experimental counterparts at the central location for all the drag models. After changing the specularity coefficient from 0.5 to 0.125 for 2.19 m/s case and 0.5 to 0.05 for 3.28 m/s case, the required bump in the vertical velocity at central location was observed for both GEW and Syamlal drag correlations. Low values of specularity coefficient produce high particle velocities in the bed as there is less loss of tangential momentum to the walls [5].

Finally, Syamlal O'Brien's drag correlation performed exceptionally well in replicating the experimental results for both the gas velocities. The reason for this realistic behaviour could be because of the consideration of the clustering effect [6] of particles in the model, unlike other correlations. Gidaspow-Ergun-Wen-Yu drag correlation performed on par with the Syamlal model at lower gas velocity. As the gas velocity was increased to 3.28 m/s, though the trend in both horizontal and vertical velocities was replicated exactly, a higher relative error than that of the Syamlal model makes it unsuitable at higher velocities.

## 4.2 BFS MICROCHANNEL – Single phase Study

The results obtained using the simpleFoam solver for all three types of microchannel designs are depicted and discussed below. Further, the results are validated against the data generated for the similar Single-phase study conducted in [4].

### 4.2.1 Result 1: Straight Inlet Microchannel – Type 1

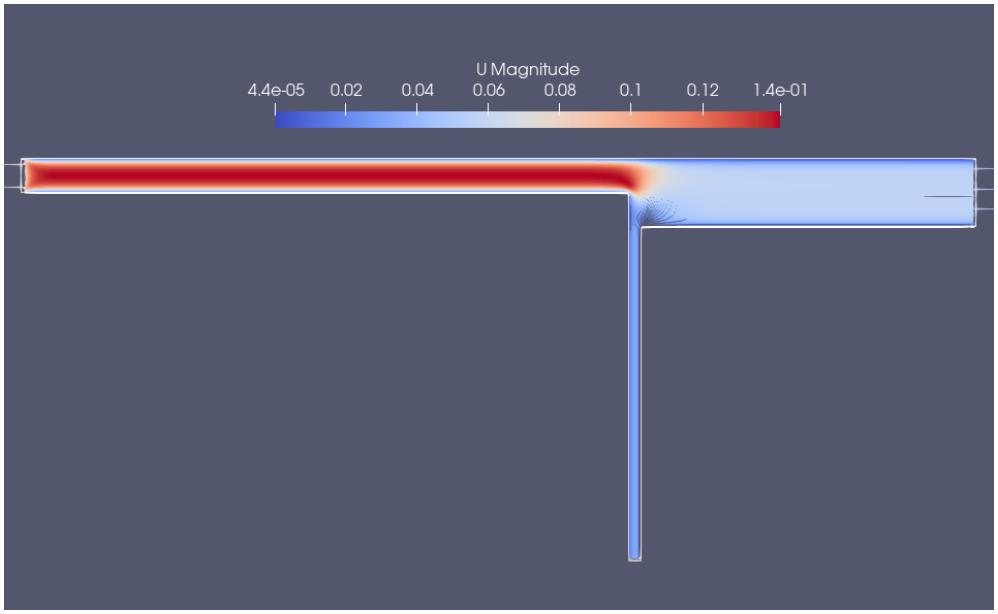


Figure 16: Velocity contour of Type I Microchannel at steady state

### 4.2.2 Result 2: Uniform Bent Inlet Microchannel – Type 2

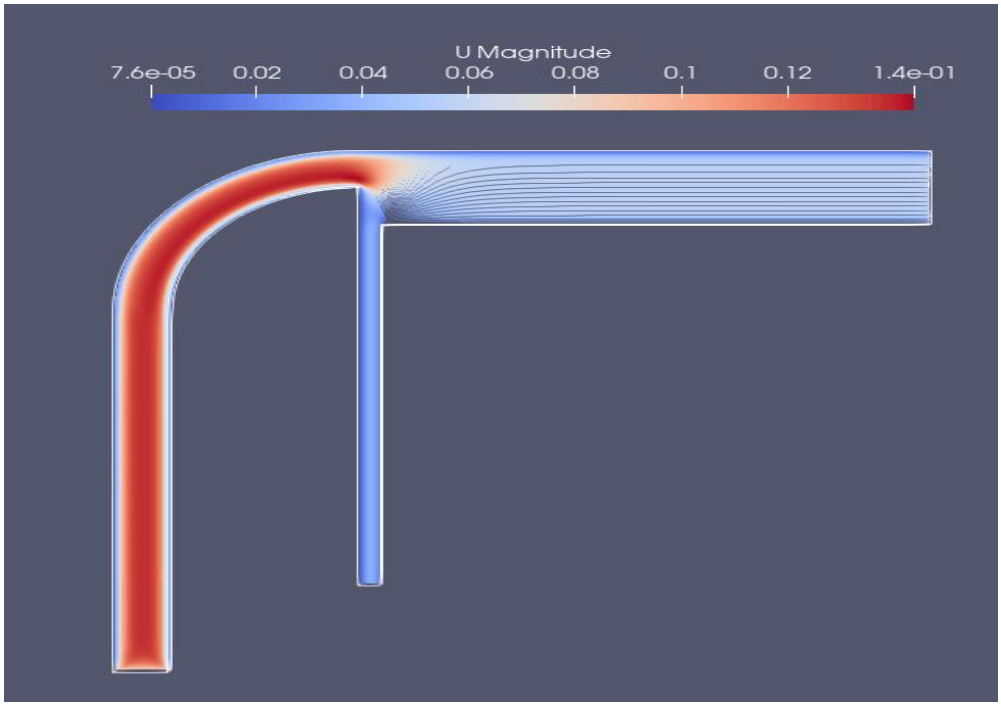


Figure 17: Velocity contour of Type II Microchannel at steady state

### 4.2.3 Result 3: Converging Bent Inlet Microchannel – Type 3 (Novel type)

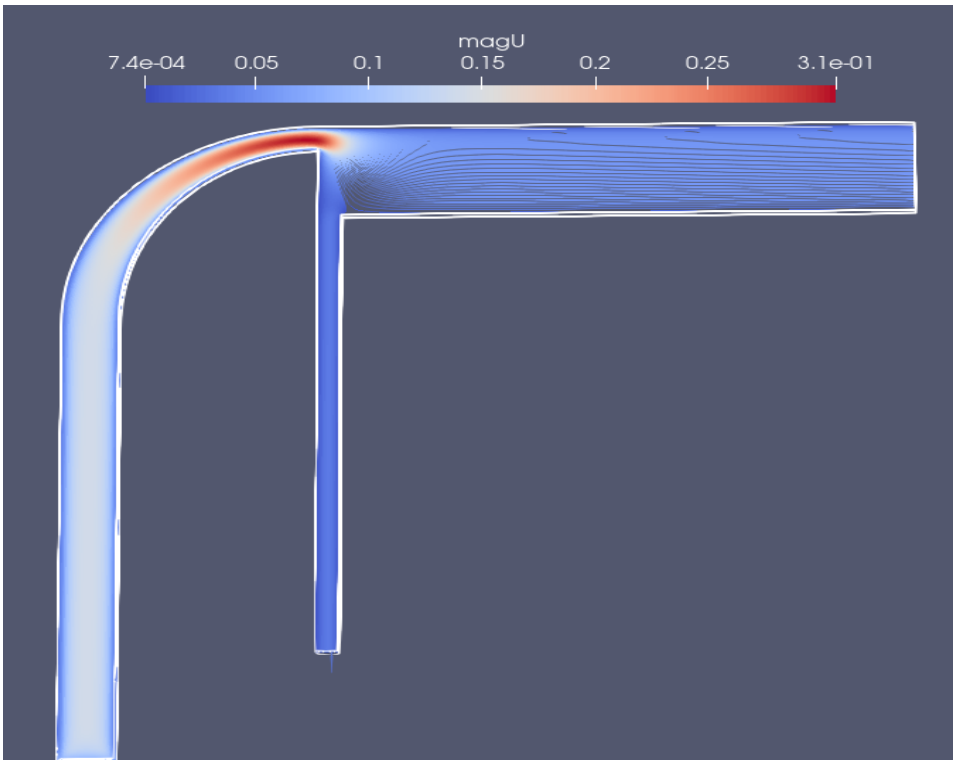


Figure 18: Velocity contour of Type III Microchannel at steady state

Two important parameters used in this Single-phase study for comparison of flow properties between microchannel design variants are:

a. Flow rate ratio ($\alpha$)
b. Minimum Radius (R)

The flow rate ratio is the ratio of volumetric flow rate in the side channel ($Q_1$) to the inlet flow rate ($Q_0$). The flow rate ratio is given by $\alpha = Q_1 / Q_0$. This parameter is obtained by averaging the velocity at the outlet of the side channel and the inlet for different microchannels. The values obtained are tabulated in Table 14.

Minimum radius (R) is considered to be the dimension of the smallest particle that can be excluded from the side channel. This is calculated by measuring the vertical distance of the last streamline entering the side channel from the bottom wall of the inlet measured. Both flow rate ratio and minimum radius are obtained by post-processing the results using the open-source visualization software, ParaView. Minimum radius of the three microchannel designs is tabulated in Table 15.

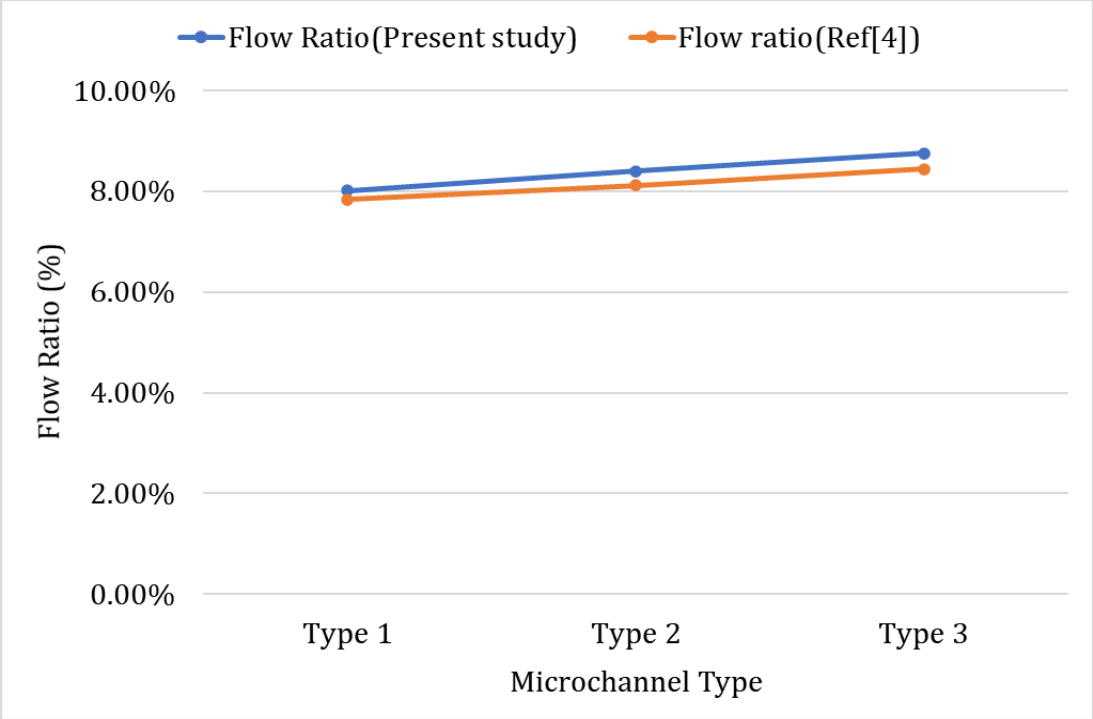


Figure 19: Flow ratio comparison

| Microchannel Type | $\alpha$ (%) | $\alpha$ (%) [4] | Error % |
|---|---|---|---|
| Type I | 8.01% | 7.83% | 2.29% |
| Type II | 8.40% | 8.11% | 3.57% |
| Type III (novel) | 8.75% | 8.44% | 3.67% |

Table 14: Error % of the flow ratio obtained in this study wrt [4]

Values of flow rate ratio and relative error percentage indicate that the results are in well agreement with those obtained in [4]. The slight deviation in the results is possibly due to the difference in mesh sizes/elements between computational domains of [4] and the ones used for this study (450k elements vs 490k elements). However, the trend was reproduced successfully where the flow rate ratios gradually increased from Type I to Type III designs. The increase in flow ratio from Type I to Type II microchannel is an indication that the centrifugal effect due to the bent design aids in elevating the quantity of plasma that is being extracted from the side channel.

We can conclude from the results that the novel Type III design has the best flow rate ratio among others because of the combination of bent and converging inlet which aids is extraction of an increased amount of plasma from the side channel.

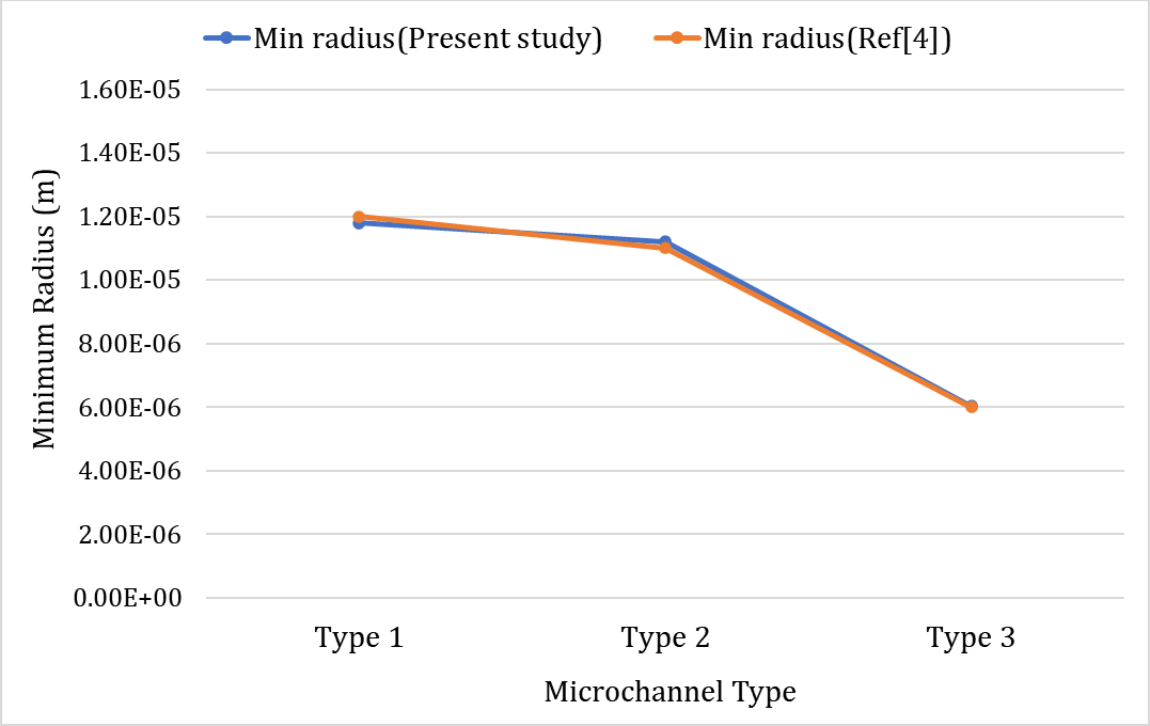


Figure 20: Minimum Radius comparison

| Microchannel Type | Minimum Radius R (μm) | Minimum Radius R (μm) [4] | Error % |
|---|---|---|---|
| Type I | 1.18E-05 | 1.20E-05 | 1.66% |
| Type II | 1.12E-05 | 1.10E-05 | 1.81% |
| Type III (novel) | 6.04E-06 | 6.00E-06 | 0.66% |

Table 15: Error % of the Minimum radius obtained in this study wrt [4]

The minimum radius (R) obtained from post-processing for each microchannel design is tabulated in Table 15 alongside the values from reference [4]. Geometry with the least minimum radius is preferred among the design variants at a length scale, as the RBCs having

a larger mean radius than the smallest minimum radius cannot enter the side channel, thereby allowing the extraction of a larger amount of plasma at a higher rate.

Type III design has the least minimum radius among other designs which makes it a potential design for enhanced plasma extraction at a higher flow rate among others.

**Multiphase Study**

### 4.2.4 Results obtained so far

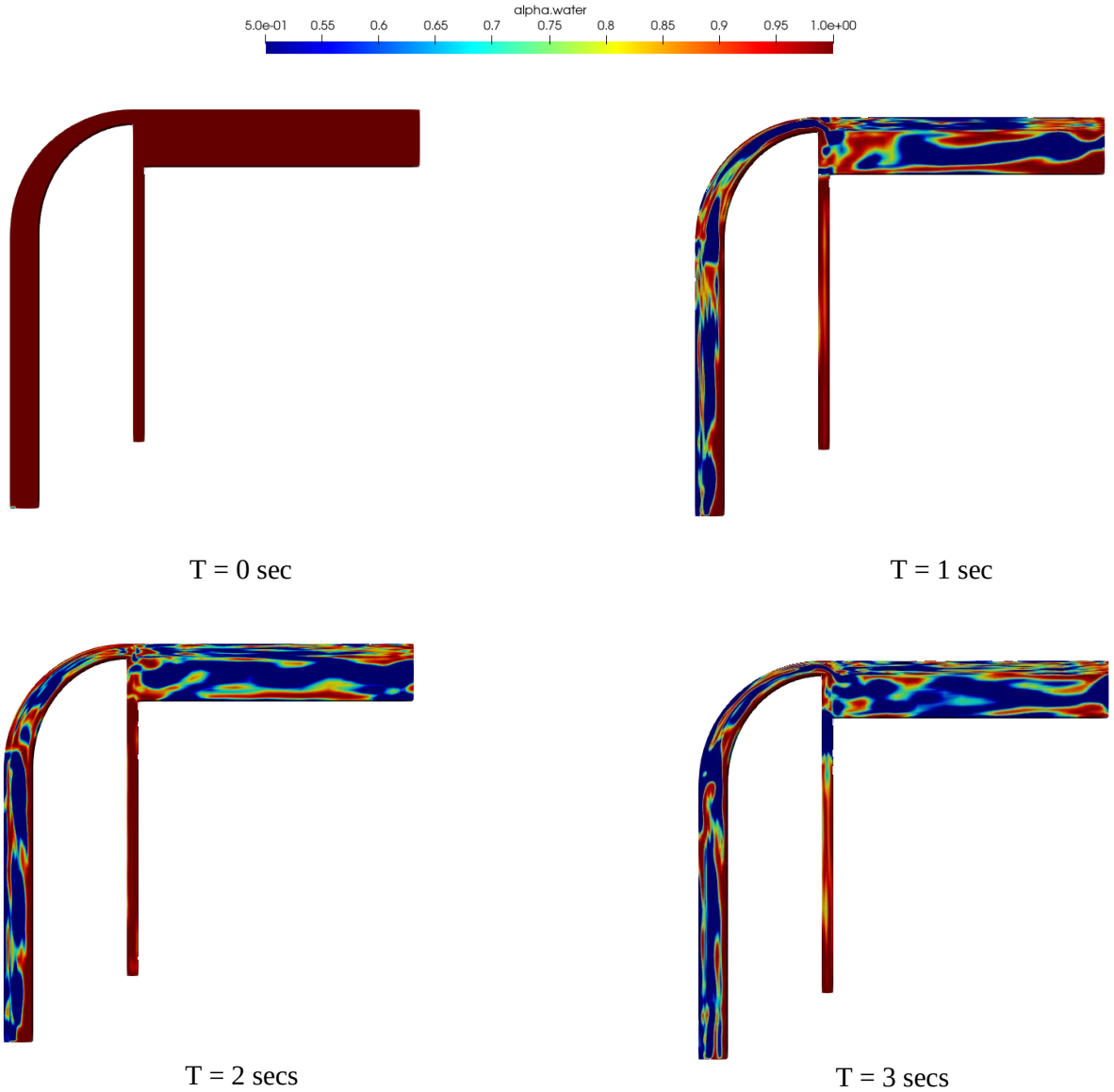


Figure 21: Contours of plasma phase fraction ($\alpha_p$) at four different timestamps

At t=0, the entire channel is filled with plasma. As time progresses, we can observe the diffusion of RBCs into the side channel whose outlet is our region of interest. Further studies include the evaluation of flow rate ratio and the quality of plasma exiting the side channel in this low haematocrit flow.

# CHAPTER 5
# CONCLUSION AND FURTHER WORK

First half of the study was conducted to identify the most reliable drag correlation for computational modelling of dispersed Multiphase flows in a Fluidized bed. The CFD results of particle velocity profiles obtained for different drag correlations were compared with the experimental data. Syamlal O'Brien drag correlation outperformed others for both the cases of superficial gas velocity, 2.19 m/s and 3.28 m/s, by accurately predicting the Mean Eulerian particle velocity distributions at various lateral locations of the fluidized bed. The Gidaspow-Ergun-Wen-Yu correlation's predictions were on par with the former for lower gas velocity of 2.19 m/s but are only satisfactory for the 3.28 m/s gas velocity case. The Gidaspow-Schiller-Naumann correlation was least accurate among the three in predicting the velocity profile but has given useful insights about the model and its operating range.

Second half of the study dealt with the Single-phase simulations of BFS microchannels. The results from all three microchannel designs from [4] are validated using the simpleFoam solver in OpenFOAM. The novel microchannel, Type III, has a flow ratio of 8.75%, highest among all other design variants. This is due to the converging bent inlet that accelerates the flow with the help of centrifugal effect due to the bend and a converging structure. Also, the minimum radius of the particles that can be excluded from the side channel is the least for the novel Type III microchannel.

The newly identified microchannel design was used for multiphase simulations of blood, wherein the RBCs and Plasma was considered as the dispersed and continuous phase respectively. From the conclusion of the fluidized bed study, Syamlal O'Brien drag closure is implemented to investigate if it gives desirable results in the Blood flow case. It can be observed from the plasma contours that the RBCs are gradually diffusing into the side channel and the fluid is not purely plasma but a combination of both the phases. Future study involves evaluating the quantity and quality of plasma exiting the side channel and comparison with other literature for low haematocrit flow.

# 6. REFERENCES

[1] H, Enwald, E. Peirano, A-E Almstedt 'Eulerian Two-Phase Flow Theory Applied to Fluidization' Int. J. Multiphase Flow, Vol. 22, Suppl, pp. 21-66, 1996

[2] National Energy Technology Laboratory (NETL). (2013, May 30). Small Scale Challenge Problem I (2013). https://mfix.netl.doe.gov/experimentation/challenge-problems/small-scale-challenge-problem-i-2013/

[3] Ding, J. and Gidaspow, D. A bubbling fluidization model using kinetic theory of granular flow. AIChE Journal 36, 523-538, 1990

[4] Ashley Melvin, Janani Srree Murallidharan, Numerical Analysis of Plasma Extraction in a Backward facing Step Microchannel using OpenFOAM, FMFP2020–152, 2020.

[5] Lungu, M., Wang, H., Wang, J., Yang, Y., & Chen, F. Two-Fluid Model Simulations of the National Energy Technology Laboratory Bubbling Fluidized Bed Challenge Problem. Industrial & Engineering Chemistry Research, 55(17), 5063–5077, 2016

[6] O'Brien, T. J. and Syamlal, M. Particle cluster effects in the numerical simulation of a circulating fluidized bed. 4th Int. Conf. on CFB, Somerset, USA, Preprint Volume, pp. 430—435, 199

[7] Johnson, P. C., & Jackson, R. Frictional–collisional constitutive relations for granular materials, with application to plane shearing. Journal of Fluid Mechanics, 176(-1), 67, 1987

[8] Khan, M. N., & Shamim, T. (2017). Influence of Specularity Coefficient on the Hydrodynamics and Bubble Statistics of an Annular Fluidized Bed Reactor. Energy Procedia, 105, 1998–2003.